TRANSACTIONS OF THE INSTITUTE OF FLUID-FLOW MACHINERY

No. 130, 2015, 57–69

KRZYSZTOF KARAŚKIEWICZ[1] and ŁUKASZ ZŁOTY

Investigations of turbulent flow through axial thrust balance holes in rotodynamic pumps

Institute of Heat Engineering, Faculty of Power and Aeronautical Engineering, Warsaw University of Technology, pl. Politechniki 1, 00-661 Warsaw, Poland

Abstract

The results of numerical investigations of flow through axial thrust balance holes in impeller of low specific speed pump were presented. The results were compared with available empirical investigations. It is a lack of numerical analyses in foregoing literature on flow through rotating holes. The issue is important for designing rotodynamic pumps. There are difficulties in solving the problem of precisely computing the flow in balance holes analytically.

Keywords: Rotodynamic pumps; Turbulent flow

Nomenclature

Δp	–	pressure difference, Pa
p	–	static pressure, Pa
d	–	hole diameter
l	–	hole length
Sh	–	Strouhal number
μ	–	flow coefficient

[1]Corresponding Author. E-mail address: krzysztof.karaskiewicz@itc.pw.edu.pl

Subscripts

[1]	–	value from measurements
s	–	value from simulation
I	–	inflow side of test bed, simulation
II	–	outflow side of test bed, simulation
d	–	pitch diameter of holes
o	–	value relates to a hole

1 Introduction

Using balance holes in rotodynamic pumps is relatively simple and effective method to reduce axial thrust. Existing recommendations for balance holes system are far from the expected precision. One can make it by trial and error but this way never guaranties the optimal result and can lead to unnecessary costs. Table 1 gathers literature recommendations for balance holes. None of them provides values of pressure drop or friction coefficient in the holes and the precise diameter of the annular seal on the impeller rear shroud.

Table 1: Literature recommendations.

No.	Author	Recommendations	Formula on pressure drop, Δp, or flow coefficient	Assessment of Arial thrust reduction
1	J. F. Gulich [4]	+	–	80–90%
2	M. Stępniewski [3]	+	+	up to 70%
3	Troskolański and Łazarkiewicz [5]	+	–	up to 75%
4	Jankowski and Kurpisz [6]	+	–	60–90%
5	A.J. Stepanoff [7]	+	–	75–90%
6	W. Jędral [2]	+	–	80–90%

A few experimental investigations of the subject are available in the literature and no numerical ones. This paper contributes into the subject of numerical simulation of turbulent flow through axial thrust balancing holes. The goal of the subject is better understanding phenomena inside the balancing holes and optimization of size, shape, number and positions of balancing holes. The influence of impeller blades is unimportant for holes characteristics so investigation is focused on impeller hub only with balancing holes.

2 Experimental investigations

Extensive tests were made on a test bed [1] simulating flow through balancing holes in OS pumps. The range of parameters was typical for that kind of pumps and as follows:

- rotation velocity $u_0 = 4.26$–17.04 m/s;
- hole diameter $d_0 = 10.0$–29.9 mm;
- hole length $l_0 = 14.1$ mm, 16.1 mm, 25.3 mm;
- average flow rate through one hole up to $v_0 = 2.5$ dm^3/s

Disks, were holes made parallel to disk axis, were shaped according to impeller hub and rotated with four different rotational speeds n = 375, 750, 1125, and 1500 rpm. The pith diameter, d_d, was equal to 218 mm.

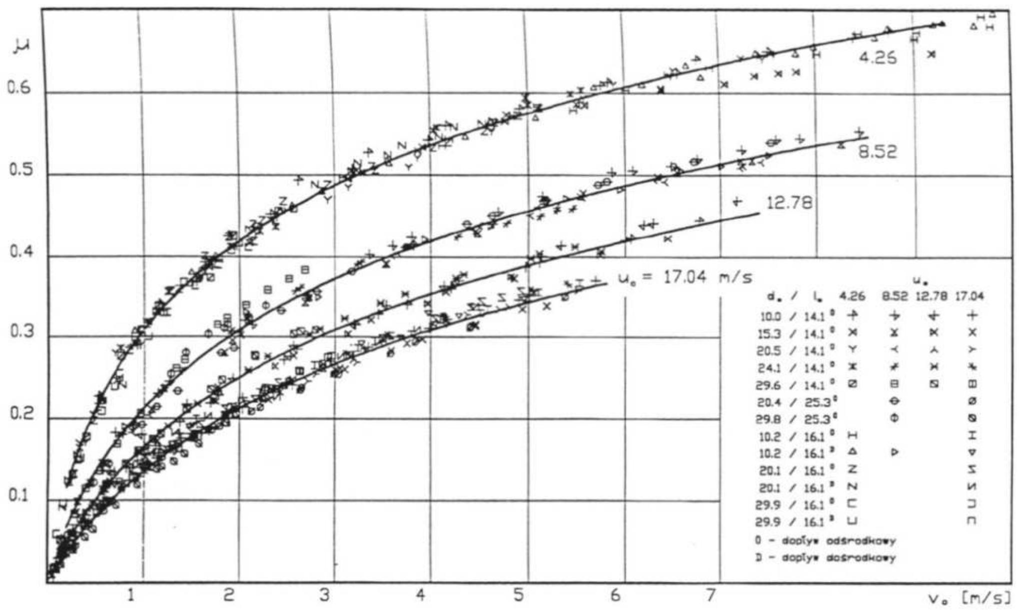

Figure 1: Relation between the flow coefficient and average flow rate through a hole for different rotation velocities [1].

The results of measurements of flow coefficient, μ, for different rotational speeds are presented on Fig. 1. The values of the flow coefficient were approximated in [1] by the following formula:

$$\mu = 0.183 \ln \left(\frac{3}{Sh} + 1 \right) , \tag{23}$$

here:

$$Sh = \frac{r_d}{v_0 t^*} = \frac{u_0}{2\pi v_0}\,, \tag{24}$$

where $t?$ denotes rotation period equal actual rotation speed in rpm divided by 60, v_0 is average flow rate through one hole. It comes from the measurements [1] that the flow coefficient does not depends on length and diameter of the holes. Maximum absolute error of the flow coefficient measurements from 1 equation was ±0.00757. Mercury manometer was used to reading difference of static pressure values from both sides of the test bed in [1].

3 Model of the test bed

The geometrical model of the tested area (flow area) is presented in Fig. 2, and the cross-sections of the model are shown in Fig. 3. The chamber in which the disk with the holes is rotating has the same dimensions in both cases of the flow, i.e., centripetal and centrifugal one. The chamber diameter equals ϕ510 mm, and the width of it equals 120 mm. The chamber in which the disk with the holes is rotating has the same dimensions in both cases of the flow, i.e., centripetal

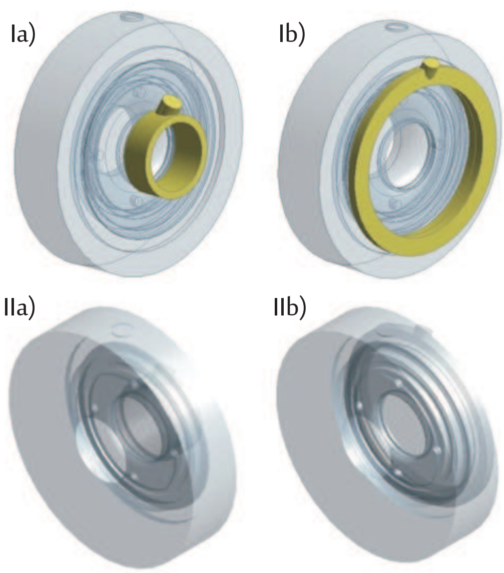

Figure 2: Geometry of flow area in test bed and symbols: I – inflow side, II – outflow side; a – centrifugal flow to holes, b – centripetal flow to holes.

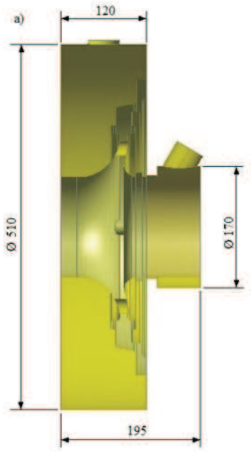

Figure 3: The cross-sections of the model for two cases a) centrifugal; b) centripetal.

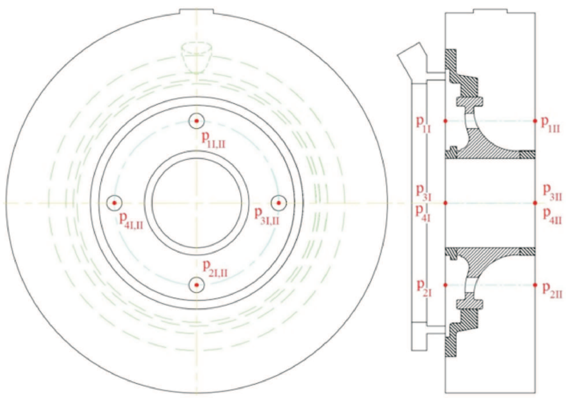

Figure 4: The positions of reading pressure points.

and centrifugal one. The chamber diameter equals ϕ510 mm, and the width of it equals 120 mm. The points of reading static pressure are presented in Fig. 4. There were four points uniformly distributed on the pith diameter on each of both sides, I – inflow, and II – outflow, respectively.

4 Meshing

In the flow region the hybrid mesh was used, structured mesh near wall regions and unstructured one in the rest of the flow area. The mesh was more dense near elements of stronger curvature. The mesh for centrifugal flow geometry is presented in Fig. 5. The parameters of the mesh for two cases, i.e., for centrifugal and centripetal flow into holes are presented in Tab. 2.

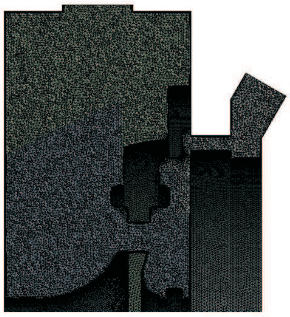

Figure 5: The mesh of flow area for centrifugal case.

Table 2: Parameters of the mesh for two cases of the flow beforethe holes.

Case of flow	Nos of nodes	Nos of elements	Average skewness	Max. skewness
centripetal flow	26 481 400	5 651 003	0.217	0.863
centrifugal flow	26 085 681	5 501 062	0.217	0.904

5 Modeling the turbulent flow

Realizable model, k-ϵ [8] was applied with scalable wall functions. Additionally for comparison SST model [9] was used for one of computed cases. As a numerical approach, second order upwind scheme was applied.

As the first boundary condition, mass flow inlet was fixed on the inlet surfaces. Arrows in Fig. 6 are located on normal directions to this surfaces and points inlet fluid direction.

As the second boundary condition, pressure outlet was fixed on the outlet surfaces. Arrows in Fig. 7 are located on normal directions to these surfaces and points outlet direction from fluid domain. For both boundary conditions turbulence

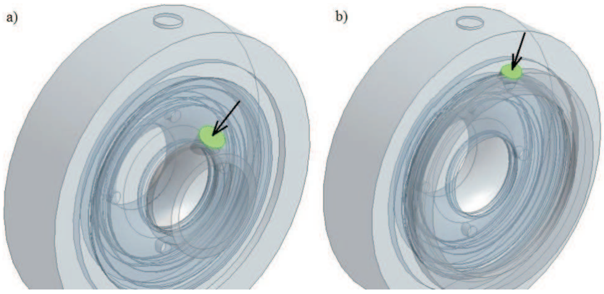

Figure 6: Inlet surfaces in case of: a) centrifugal, and b) centripetal flow.

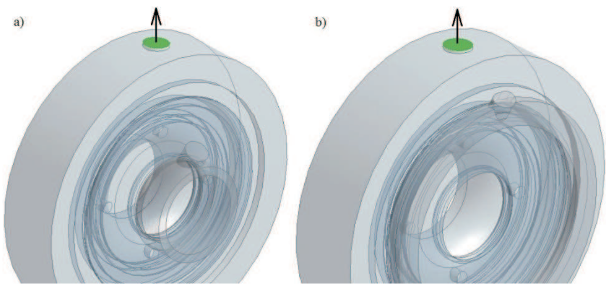

Figure 7: Outlet surfaces in case of: a) centrifugal, and b) centripetal flow.

intensity 5% was assumed. Frozen rotor approach was applied with rotating frame surface in the middle between rotating and stationary walls.

6 Results of computations

Different variants of computed cases were labeled by four elements:

1. Type of flow into holes – Cf/Cp (Centrifugal/Centripetal),
2. Rotational speed od disk,
3. Diameter of holes,
4. Lenght of holes,

for example Cf/375/20.1/14.1 means centrifugal flow with disk rotational speed $n = 375$ rpm and hole diameter $d_0 = 20.1$ mm , hole length $l_0 = 14.1$ mm.

In Tabs. 3 to 10 the four values of the static pressure around pich diameter on both sides of the disk are presented and their difference is compared with measured pressure drop in four positions. Table 3 shows a static pressure values for flow through the holes without rotations.

Table 3: The pressure values computed and measured for k-ϵ model in the case of no flow with uncertainties of computed results.

Cp/0/20.1/16/1			
No.	p_I[Pa]	p_{II}[Pa]	Δp_s [Pa]
1	34 470	22 349	12 121
2	36 980	25 727	11 858
3	28 878	17 020	11858
4	26 337	16 260	10 077
		mean Δp_s:	11 327

Table 4: The pressure values computed and measured for k-ε model.

Cp/375/20.1/16.1			$\Delta p_{[1]}$=16 492 Pa	
No.	p_I[Pa]	p_{II}[Pa]	Δp_s [Pa]	Uncertainty[%]
1	19 583	3 210	16 373	0.7
2	21 279	3 412	17 867	8.3
3	20 635	3 465	17 170	4.1
4	20 882	3 248	17 634	6.9
Mean values of Δp_s and uncertainty:			17 261	5

Table 5: The pressure values computed and measured for SST model.

Cp/375/20.1/16.1			$\Delta p_{[1]}$=16 492 Pa	
No.	p_I[Pa]	p_{II}[Pa]	Δps [Pa]	Uncertainty[%]
1	20 164	3 693	16 471	0.1
2	21 758	3 550	18 208	10.4
3	21 263	3 440	17 823	8.1
4	20 771	3 654	17 117	3.8
Mean values of Δp_s and uncertainty:			17 405	5.5

The computations were carried out also for SST model. For the same case the uncertainty of SST model vs. k-ε model (Tabs. 5,7) is visibly larger so that model was not applied for farther computations. In Tab. 10 are presented a values of $y+$ on the rotating walls, because this parameter achieved maximum numbers there.

Table 6: The pressure values computed and measured for k-ε model.

Cp/1500/20.1/16.1			$\Delta p_{[1]}$=87 136 Pa	
No.	p_I[Pa]	p_{II}[Pa]	Δp_s [Pa]	Uncertainty[%]
1	65 036	-19 534	84 570	2.9
2	69 121	-18 221	87 341	0.2
3	66 984	-19 442	86 425	0.8
4	68 064	-17 732	85 796	1.5
Mean values of Δp_s and uncertainty:			86 033	1.4

Table 7: The pressure values computed and measured for SST model.

Cp/1500/20.1/16.1			$\Delta p_{[1]}$=87 136 Pa	
No.	p_I[Pa]	p_{II}[Pa]	Δp_s [Pa]	Uncertainty[%]
1	54 493	-18 384	72 877	16.4
2	68 555	-19 569	88 124	-1.1
3	60 701	-19 586	80 287	7.9
4	63 766	-16 589	80 355	7.8
Mean values of Δp_s and uncertainty:			80 411	8.3

Table 8: The pressure values computed and measured for k-ε model.

Cf/750/20.5/14.1			$\Delta p_{[1]}$=30 030 Pa	
No.	p_I[Pa]	p_{II}[Pa]	Δp_s [Pa]	Uncertainty[%]
1	25 662	-2 016	27 678	7.8
2	25 187	-1 729	26 916	10.4
3	24 479	-2 050	26 529	11.7
4	25 121	-1 586	26 707	11.1
Mean values of Δp_s and uncertainty:			26 958	10.2

The mesh was not changed for the centrifugal flow although different flow field structure with different boundary layers was achieved. It could be the possible reason of larger uncertainty for that case comparing to centripetal flow.

Table 9: The pressure values computed and measured for k-ε model.

Cf/1500/20.5/14.1			$\Delta p_{[1]}$=30 030 Pa	
No.	p_I[Pa]	p_{II}[Pa]	Δp_s [Pa]	Uncertainty[%]
1	30 173	-24 185	54 358	10.8
2	30 103	-23 573	53 676	11.9
3	29 792	-24 355	54 147	11.1
4	30 242	-23 157	53 399	12.3
Mean values of Δp_s and uncertainty:			53 895	11.5

Table 10: Computed values of dimensionless wall distance.

Case	Range of y+ on moving walls	
	min	max
Cp/375/20.1/16.1 [k-ε]	6	51
Cp/375/20.1/16.1 [SST]	3	52
Cp/1500/20.1/16.1 [k-ε]	11	142
Cp/1500/20.1/16.1 [SST]	10	148
Cf/750/20.5/14.1 [k-k-ε]	6	78
Cf/1500/20.5/14.1 [k-ε]	7	140

Contours of static pressure in hole for different cases shows Fig. 8. The static pressure is not uniform in the hole and the nonuniformity is the more the larger rotational speed of the disk. For the same rotational speed the pressure fields in the hole differ in the case of centrifugal and centripetal flows.

The stream lines of the water flowing through the holes are presented in Fig. 9. The important change in flow pattern occurs when the rotational speed of the disk increases. In the upper part of the hole a secondary flow appears the bigger the grater rotational speed. The existing vortex obstructs a part of the hole and make harder the flow through it.

7 Conclusions

Upper part of each hole is blocked by the vortex the larger the higher the rotational speed of the disk. The velocity of vortex in balancing hole is comparable to the speed of the hole but of opposite direction. The average flow through the hole

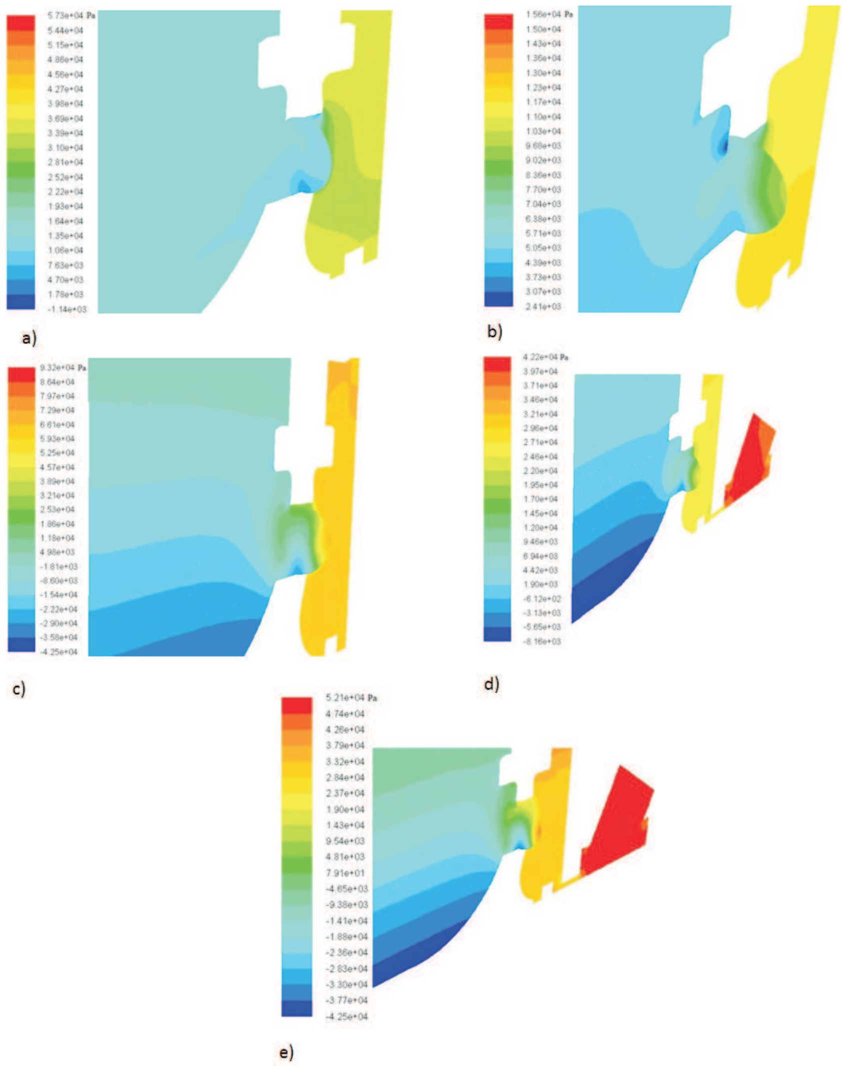

Figure 8: Countours of static pressure for different cases: a) Cp/0/20.1/16/1, b) Cp/375/20.1/16.1, c) Cp/1500/20.1/16.1, d) Cf/750/20.5/14.1, e) Cf/1500/20.5/14.1.

is lower than it would be without the vortex structure. The water right behind the hole turns back decreasing the average flow.

Farther investigations should be done to check the influence of rotational speed on flow patterns inside the hole and possible remedies to limit the appearance of vortex, i.e., some elements to suppress it.

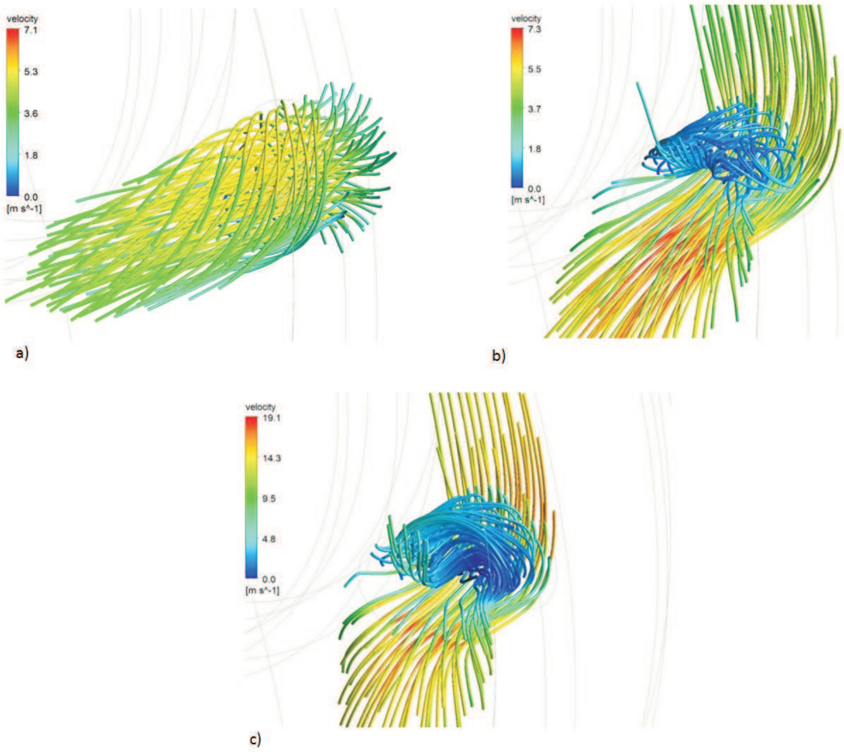

Figure 9: Stream lines in the hole for different cases: a) Cp/0/20.1/16.1, b) Cp/375/20.1/16.1, c) Cp/1500/20.1/16.1.

Different meshing should also be checked for centrifugal flow case where uncertainties are significantly larger than for centripetal flow case. The numerical results for centripetal flow case are in good agreement with empirical data.

Received 10 November 2015

References

[1] Wilk A.: *Flow rate coefficient through the exculpatory holes in the rotodynamic pump*. PhD thesis, Silesian University of Technology in Gliwice, Gliwice 1998.

[2] Jędral W.: *Rotodynamic pumps*. WN PWN Warsaw 2001.

[3] Stępniewski M.: *Pumps.* WNT, Warsaw 1985.

[4] Gülich J. F.: *Centrifugal Pumps.* Springer-Verlag, Berlin Heidelberg 2008.

[5] Łazarkiewicz S., Troskolanski A.: *Rotodynamic pumps.* 3rd Edn., Warsaw 1973.

[6] Jankowski Z., Kurpisz Ł.: *Balancing of axial forces in rotodynamic pumps.* ITC Information Bulletin No. **34**, Warsaw University of Technology, Warsaw 1972.

[7] Stepanoff, A.J.: *Centrifugal and Axial Flow Pumps: Theory, Design, and Applications.* Wiley, New York 1957.

[8] Shih T.-H., Liou W.W., Shabbir A., Yang Z., and Zhu J.: *A new – eddy-viscosity model for high Reynolds number turbulent flows – Model development and validation.* Computers Fluids **24**(1995), 3, 227–238.

[9] Menter F.R.: *Two-equation eddy-viscosity turbulence models for engineering applications.* AIAA J. **32**1994, 1598–1605.